Mitigation of gravity-induced distortions of binder-jetting components during rotational sintering

Downloaded from: https://research.chalmers.se, 2024-07-10 14:22 UTC

Citation for the original published paper (version of record):
Grippi, T., Torresani, E., Cabo Rios, A. et al (2024). Mitigation of gravity-induced distortions of binder-jetting components during rotational
sintering. Additive Manufacturing Letters, 10. http://dx.doi.org/10.1016/j.addlet.2024.100215

N.B. When citing this work, cite the original published paper.

research.chalmers.se offers the possibility of retrieving research publications produced at Chalmers University of Technology.
It covers all kind of research output: articles, dissertations, conference papers, reports etc. since 2004.
research.chalmers.se is administrated and maintained by Chalmers Library

(article starts on next page)

Additive Manufacturing Letters 10 (2024) 100215

Contents lists available at ScienceDirect

Additive Manufacturing Letters

journal homepage: www.elsevier.com/locate/addlet

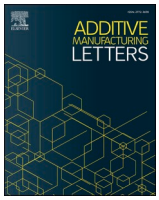

Short Communication

Mitigation of gravity-induced distortions of binder-jetting components during rotational sintering

Thomas Grippi [a,*], Elisa Torresani [a], Alberto Cabo Rios [b], Andrii L. Maximenko [a], Marco Zago [c], Ilaria Cristofolini [c], Alberto Molinari [c], Rajendra K. Bordia [d], Eugene A. Olevsky [a,e]

[a] Mechanical Engineering, San Diego State University, San Diego, USA
[b] Department of Industrial and Materials Science, Chalmers University of Technology, Gothenburg, Sweden
[c] Department of Industrial Engineering, University of Trento, Trento, Italy
[d] Department of Materials Science & Engineering, Clemson University, Clemson, USA
[e] NanoEngineering, University of California, La Jolla, San Diego, USA

ARTICLE INFO

Keywords:
Rotating sintering
Deformation
Sintering
Finite element methods
Binder jetting

ABSTRACT

Using theory and simulations, the challenge of gravity-induced distortions during sintering is addressed and a mitigation strategy is proposed. Based on the continuum theory of sintering, the finite element simulation demonstrates the advantages of a rotating furnace to counteract gravity forces during sintering. Its application for stainless steel hollow parts produced by additive manufacturing (binder jetting) is demonstrated, numerically, for reliable industrial production of complex shapes. Sintering a tube in a very slow rotating motion exhibits an improvement in the final deformation ratio compared to a conventional sintering process.

The same concept has been adapted for higher furnace revolution speeds and the centrifugal force is now surpassing the effects of gravity. An extended study of sintering under microgravity for space-borne applications is also widely depicted with the same model. Indeed, it shows the possibility of reproducing Earth's sintering conditions at places where gravity is insufficient to provide acceptable densification and shape conservation during sintering.

1. Introduction

Processes combining heat treatment in a rotating frame have been widely documented and have various applications in the industry. The rotational molding or spin casting of polymers is one of the examples, hollow parts like tanks or containers are produced via the heating and the slow rotation, around 2 axes, of a plastic powder in a mold [1–3]. In foundry, the term "rotating furnace" refers to the use of rotating kilns for the mixing and segregation of granular materials [4,5]. The term can also refer to the manufacturing of parabolic mirrors for optical telescopes, by pouring a molten glass that solidifies on a rotating parabolic mold [6]. However, the combination of a rotary motion with a thermal treatment for free sintering homogenization has not been investigated. This paper presents the simulation of sintering in a rotating furnace.

Amongst factors that lead to distortion of a part during its free sintering, gravity is one of the most important especially for heavy metal powders [7–10]. This paper focuses on the sintering of parts produced by binder jetting which is an important powder-spread-based additive manufacturing technology [11,12]. The simulation of sintering for binder-jetted additively manufactured green compacts is needed because of the unique microstructure of the additively manufactured component leading to anisotropic shrinkage [13–15]. Sintering shrinkage and structural analysis of parts derived from these green bodies reveal that an initial anisotropic layered structure typically results in shape distortion and final material property anisotropy. Advancements in computer tomography enable detailed analysis of powder bed structure evolution during BJ processing and highlight the periodic density fluctuation mainly in the build-up direction [16]. The authors of the latter study have reported 1.6 % initial relative density fluctuation in the build-up direction with peaks separated by ~ 42 μm, although minor deviations from isotropy can be observed in other directions as well [11, 14].

The focus of this work is the exploration of mitigating such problems through the conceptualization of a novel process. In this context, the attenuation of gravity-induced distortion will focus on the FEM simulation of the sintering of a simple hollow cylindrical part attached to a

* Corresponding author at: Powder Technology Laboratory, Mechanical Engineering, San Diego State University 5500 Campanile Dr, San Diego, CA 92182, USA.
E-mail address: tgrippi@sdsu.edu (T. Grippi).

https://doi.org/10.1016/j.addlet.2024.100215
Received 7 March 2024; Received in revised form 19 April 2024; Accepted 21 April 2024
Available online 26 April 2024
2772-3690/© 2024 The Author(s). Published by Elsevier B.V. This is an open access article under the CC BY license (http://creativecommons.org/licenses/by/4.0/).

rotating frame. The study is based on the continuum theory of sintering [17] and the framework detailed by Rios et al. [18–20] for the sintering of stainless steel 316 L produced by the binder jetting process.

2. Sintering model and simulation of rotation furnace

The sintering process is defined by the main constitutive equation from Skorokhod-Olevsky continuum theory of sintering [16]:

$$\sigma_{ij} = 2\eta_0\left[\varphi\dot{\varepsilon}_{ij} + \left(\psi - \frac{1}{3}\varphi\right)\dot{\varepsilon}\delta_{ij}\right] + P_L\delta_{ij} \quad (1)$$

Where σ_{ij} the stress tensor (Pa), represents the externally applied stress, η_0 is the shear viscosity of the fully dense material (Pa·s), φ and ψ are respectively normalized shear and bulk viscosity moduli, $\dot{\varepsilon}_{ij}$ is the strain rate tensor (s^{-1}), $\dot{\varepsilon}$ is the first strain rate tensor invariant (s^{-1}), corresponding to the volumetric shrinkage, δ_{ij} is the Kronecker delta and P_L is the effective sintering stress (Pa).

φ, ψ and P_L can be expressed as a function of porosity, θ, with modified Skorokhod-Olevsky model and constitutive parameters identified for SS136L by Cabo Rios et al. [20]

$$\varphi = (1-\theta)^2 \quad (2)$$

$$\psi = \frac{2}{3}\frac{(1-\theta)^{11.548}}{\theta^{0.642}} \quad (3)$$

$$P_L = \frac{6\alpha(1-\theta)^2}{G} \quad (4)$$

With the surface tension α=1.2 J/m^2, the initial particle size G_0=8·10^{-6} m as expressed in the latter cited article. On its side, for this preliminary study the initial density is considered uniform with a mean value of 4.38 g/cm^3 (54.75 % relative density), The generalized expression of the gravity as an external load is [21]:

$$\nabla_j\sigma_{ij} = -(1-\theta)\rho_{th}\vec{g} \quad (5)$$

The viscosity η_0 is expressed as:

$$\eta_0 = A_0 T\exp\left(\frac{Q}{RT}\right) \quad (6)$$

With A_0 the pre-exponential factor (Pa·s·K^{-1}), Q the apparent activation energy of sintering (kJ/mol), R the universal gas constant, T the temperature (K)

A δ-ferrite phase transition in SS316L around 1316°C (1581 K), implies that in the model, the activation energy changes from Q_1=217.250 kJ/mol to Q_2=1182.176 kJ/mol and the pre-exponential factor changes from A_{0_1}=2.502 Pa·s·K^{-1} to A_{0_2}=4.599e-32 Pa·s·K^{-1} [22]

The grain growth is also modeled with the following expression [23]:

$$\frac{dG}{dt} = \frac{k_0}{3G^2}\left(\frac{\theta_c}{\theta+\theta_c}\right)^{\frac{3}{2}} exp\left(\frac{-Q_G}{RT}\right) \quad (7)$$

With the identified preexponential term k_0 =2.97·10^{-22} m^3·s^{-1}, the apparent grain growth activation energy Q_G =164.8 kJ·mol^{-1} and the critical porosity θ_c = 5.20 %. Finally, the thermal cycle follows a heating rate of 35 K/min from 773.15 K to 1283.15 K and 1.5 K/min from 1283.15 K to 1658.15 K and with a temperature holding of 220 min at 1658.15 K.

Two sintering configurations are considered for the conceptualization of the rotating motion. First, one might conceive the part rotating around its principal axis, surrounded by a fixed heating frame (schematically shown in Fig. 1 a.). Then, as a second concept, the motion of the part could be made by clamping it to a rotating cylindrical frame with a central fixed rod heater (Fig. 2 b.). This second configuration is

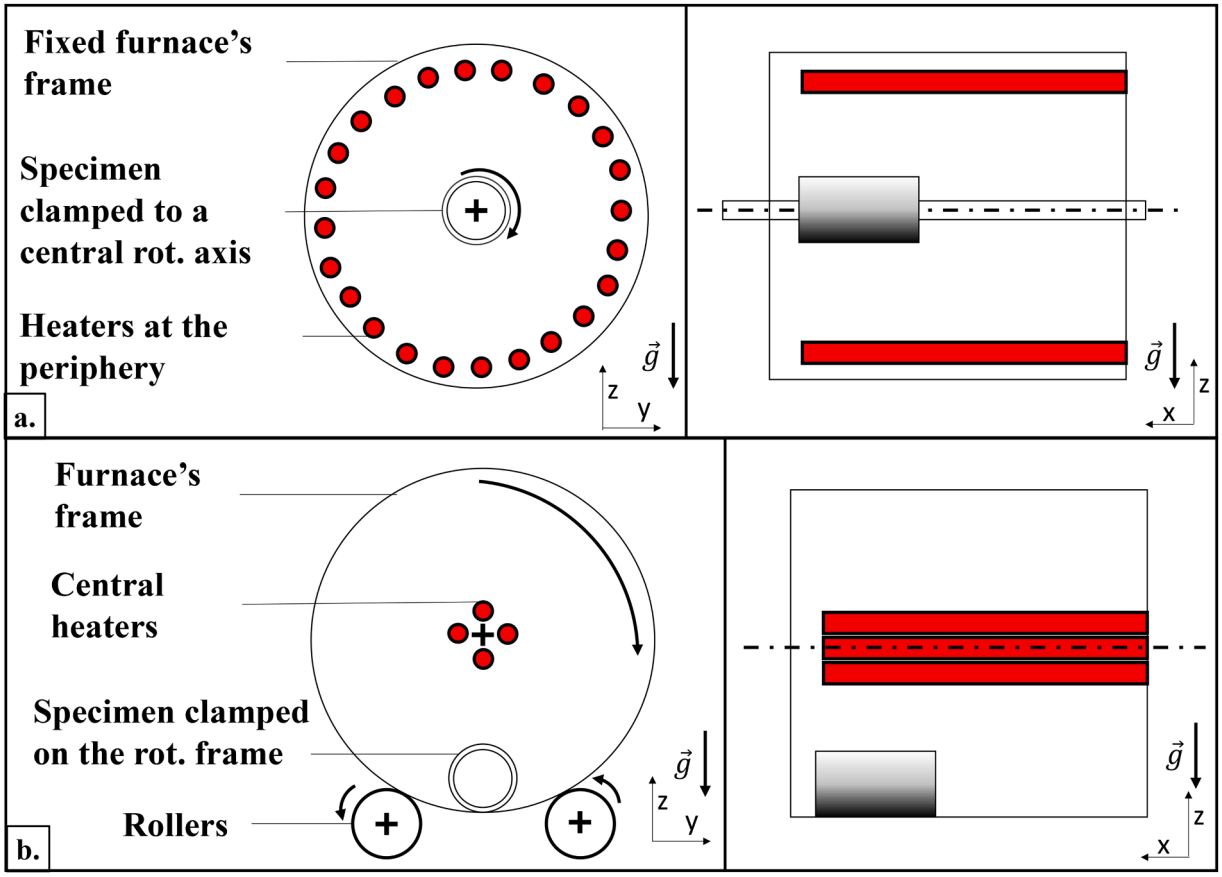

Fig. 1. Two rotating concepts with the part rotating on a transverse axis (a.) and the part clamped to a rotating frame (b.).

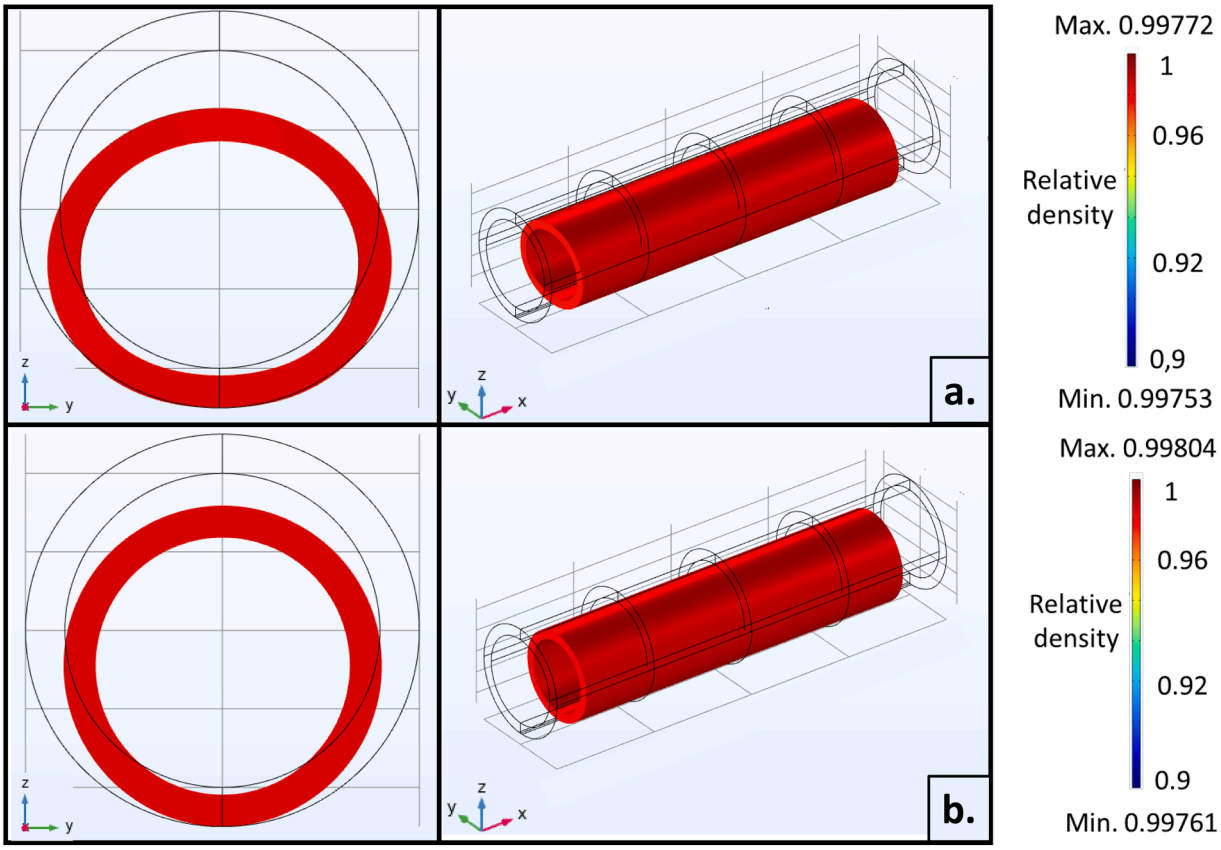

Fig. 2. Finite element sintering simulation of hollow cylinder sintered in fixed configuration (a.), and in a slow rotating furnace (b.).

explored in this article as the addition of centrifugal forces in the computation opens this model for new applications, where these centrifugal forces are used as supplementary driving forces for sintering.

By incorporating the sintering model in COMSOL™ Multiphysics software, the user interface allows the modulation (in direction and magnitude) of the gravity's application on the part and therefore, it is possible to add centrifugal forces. The addition of these 2 modules (gravity and centrifugal) to the original sintering model permits the simulation of sintering in a rotating furnace. The sintering of a simple hollow cylinder (ø10xø8 × 40 mm) is computed using the parameters presented in Section 2. The finite element model's boundary conditions are defined as follows, the contact of the cylinder with the support plate is defined as a planar surface fixed toward the z-axis, and one corner point of this surface is both fixed toward x and z. Finally, the center point on the edge segment of this latter corner is fixed toward the x, y, and z-axis.

The hollow cylindrical specimen is oriented with its height toward the x-axis and centered at $(0,\ 0,\ 0)$. The rotating motion is oriented around this same axis in the global cartesian coordinate system. The rotating frame is defined with the rotation axis base point positioned at $(0,\ 0,\ 0.2)$. With these conditions, the model reproduces the sintering of the part placed on the internal surface of a cylindrical frame of a diameter 0.4 m.

The general expression of the centrifugal acceleration embedded in the software is given by:

$$a_{cen} = \omega^2 \cdot R_i \tag{8}$$

With ω (rad·s^{-1}) the rotation speed and R_i (m) the radial distance between the base point and the geometry of the specimen. In addition, the application of gravity in the global cartesian coordinate system is now expressed as a function of the time and rotation speed:

$$\overrightarrow{g} = -g \begin{pmatrix} 0 \\ \sin\left(\frac{t\omega}{60}\right) \\ \cos\left(\frac{t\omega}{60}\right) \end{pmatrix} \tag{9}$$

Therefore, the equilibrium Eq. (5) can be rewritten with the incorporation of the gravitational and centrifugal forces to the model as:

$$\nabla_j \sigma_{ij} = (1-\theta)\rho_{th}\vec{g} + (1-\theta)\rho_{th}\overrightarrow{a_{cen}} \tag{10}$$

Injecting this latter equation (instead of Eq. (5)) into the model presented in Section 2, accounts for the effect of both gravitational and centrifugal forces on shape distortion during sintering.

3. Results and discussion

3.1. Influence of slow rotation speed

In this section, the shape of the part sintered freely without rotation is compared to the same part simulated in the rotating furnace. As presented above in Fig. 1, the study focuses on only sintering configuration "*the part clamped to a rotating frame*". Rotation speed is set to 1 revolution per 60 min. This very slow rotation speed makes the centrifugal force for the computation negligible. The variable application of gravity on the geometry is now the only component that influences the resulting slumping of the part at high temperatures.

The comparison between computation results at the final time of sintering ($t = 750$ min) shows that although both parts can fully densify up to 0.99 relative density, the fixed part shows higher slumping (Fig. 2). In Fig. 2, the original shape is shown with grey lines and the sintered shape in red color. This visualization is confirmed by the graphics in Fig. 3 where the evolutions of 5 different diameters as a function of the

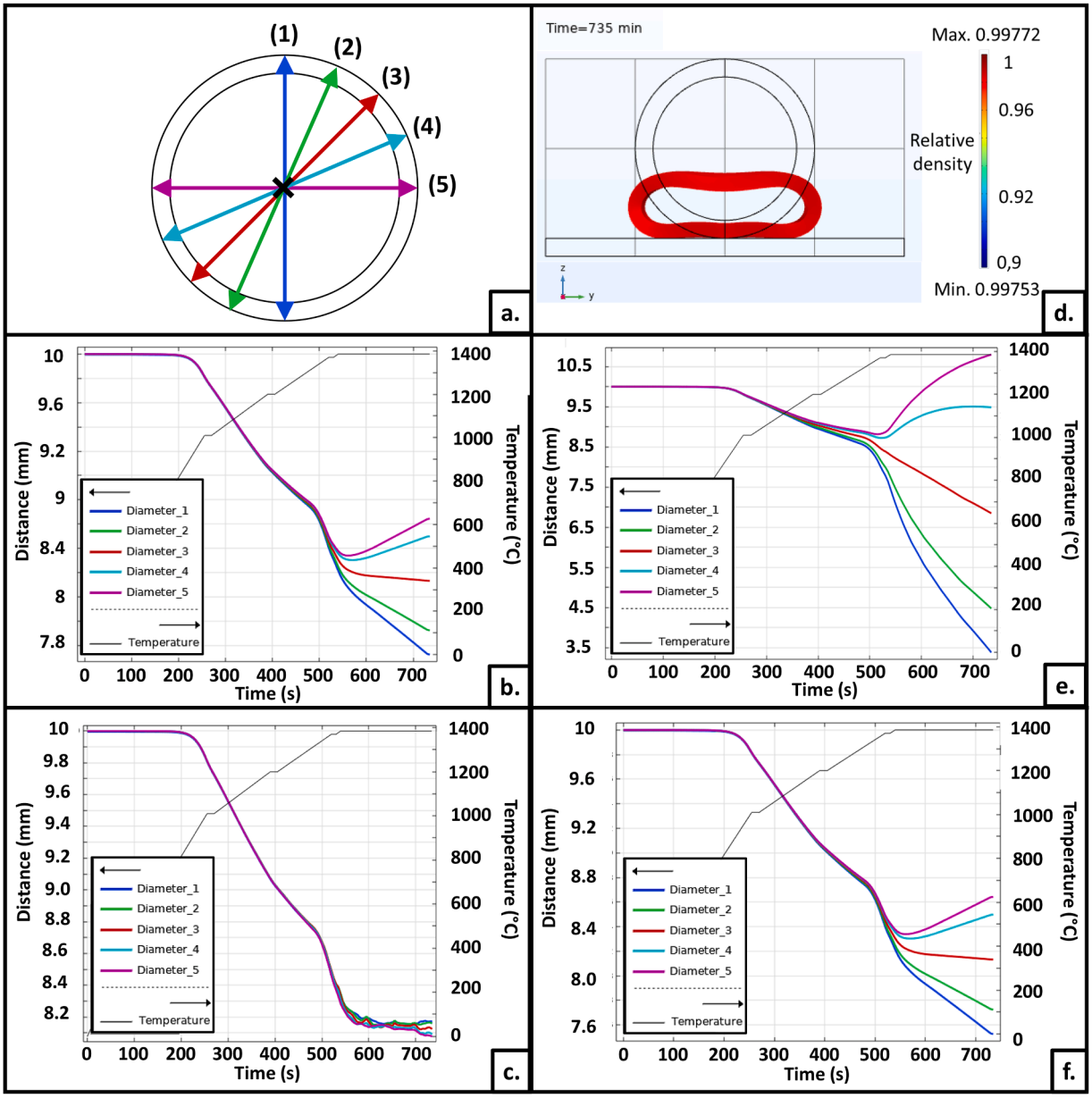

Fig. 3. (a): Schematic of the location of the five diameters used to quantify shape distortion; (b) the evolution of the five diameters as a function of temperature and time for sintering without rotation (effect of gravity only); (c) the evolution of the five diameters as a function of temperature and time for sintering at low rotation speed (1 revolution per 60 min);(d) final shape of a cylinder sintered under high rotation speed (3.6 rev/*sec*); (e) the evolution of the five diameters as a function of temperature and time for sintering at high rotation speed (3.6 rev/*sec*); (f) the evolution of the five diameters as a function of temperature and time for sintering at high rotation speed(1.1 rev/*sec*) in microgravity environment.

sintering time are plotted. (Fig. 3b for the fixed part and Fig. 3c for the part rotating at low speed). The final deformation ratio is calculated by dividing the smallest with the largest diameter, respectively (1) and (5) in Fig. 3b, a value close to unity indicates a more uniform cylinder. The part sintered freely has a deformation ratio of 0.86, whereas the configuration with the rotating furnace (Fig. 3c) has a deformation ratio of 0.99. Slow revolution at high temperatures, where the viscosity of the material is the lowest, but the density is high, allows a homogenization of the distribution of the gravity load on the part and leads to a more uniform shape retention. The simulation shows the benefits of sintering in a rotating furnace to mitigate the effect of gravity on the sintering of binder jetted parts.

3.2. *Influence of high rotation speed*

Due to the independent effect of centrifugal and gravitational forces, it is possible to do the sintering simulations with different speeds. With a higher rotating speed, the part is subject to an additional centrifugal force that would not be negligible anymore. Hence, the part is subjected to a unidirectional pressure that is directed radially in the cylindrical coordinate system.

For direct comparison, the same geometry as the one considered above is simulated but at a higher rotation speed (3.6rev/*sec*). The results are presented in Fig. 3d and 3 e. As can be seen, this part has significantly higher distortion than either the fixed sample or the one rotating at low speed. In this case, the deformation ratio decreases to 0.33. This simulation shows that rotation during sintering can also be used to change the shape of the sintering part.

The development of such technology is interesting for the sintering in the context of low gravity, for example in space, on the Moon or on Mars. The hypothesis on ideal free sintering under micro-gravity showing no distortion has been recently refuted [8,24]. In low gravity conditions, the lack of buoyancy forces prevents pore removal, and as pores coalesce there is distortion from swelling. Additionally, there is not sufficient grain compression, leading to incomplete densification. For these reasons, while gravity does not contribute to distortion, the effects of removing gravity are just as detrimental to shape fidelity after sintering

The rotation speed needed to simulate the effect of the gravity, during sintering in a rotating furnace under microgravity, can be calculated by equating the centrifugal and gravitational forces given be Eqs. (8) and (9). This results in a rotation speed of:

$$\omega = \sqrt{\frac{g}{R_i}} \tag{11}$$

With $R_i = 0.2$ m, the calculated rotation speed is 1.1 rev/*sec*. The simulation in Fig. 3f., presents a no-gravity computation but a frame rotation speed of 1.1 rev/*sec*. As anticipated, Fig. 3f. shows the same results as Fig. 3b. the original sintering configuration under gravity without rotation. Hence, controlling the rotation speed of the furnace demonstrates the potential of such technology as an answer to problems related to the free sintering of complex shapes under microgravity. Future spaceborne development objectives would be not to replicate exact Earth's condition, where we observe slumping, but to optimize the rotation speed, apply sufficient grain compression to initiate the sintering at the early stages of sintering, and then slightly reduce this rotation speed at high temperatures/low viscosity of the material to avoid the slumping due to centrifugal forces.

4. Conclusion

The study presented depicts the simulation of a novel technology to mitigate the problems of shape distortions during sintering. At high temperatures the viscosity of stainless steel is low enough that gravity has an effect and leads to shape distortion in normal sintering.

From a finite element method sintering model of stainless steel 316 L based on the continuum theory of sintering, it is possible to model a part's densification and behavior during the heating process. The simulation leads to quantification of the shape distortion during sintering under gravity. At low rotation speed (1 revolution per 60 min), the centrifugal forces compensate for the fixed direction gravitational force leading to an almost undistorted sintered cylinder (the ratio of the minimum to maximum diameter for the sintered sample of 0.99 compared to 0.86 for a non-rotating sample). Of course, the exact speed needed will depend on the geometry, the material being sintered, and the thermal history. The simulation provides a way to estimate the needed speed.

At high rotation speed (in the case presented here of 3.6 rev/*sec*), the centrifugal force dominates and leads to a significant shape distortion (deformation ratio of 0.33). The calculations have also provided a potential pathway to overcome some of the problems associated with sintering under microgravity. By sintering in a rotating furnace at a lower speed (1.1 rev/*sec*), the centrifugal force can be used to provide controlled uni-directional pressure and thus will help to overcome the problems associated with sintering under microgravity (in space) or low gravity on Moon or Mars)

CRediT authorship contribution statement

Thomas Grippi: Writing – review & editing, Writing – original draft, Software, Conceptualization. **Elisa Torresani:** Writing – review & editing, Supervision, Conceptualization. **Alberto Cabo Rios:** Writing – review & editing, Software. **Andrii L. Maximenko:** Writing – review & editing, Supervision, Conceptualization. **Marco Zago:** Writing – review & editing. **Ilaria Cristofolini:** Writing – review & editing. **Alberto Molinari:** Writing – review & editing. **Rajendra K. Bordia:** Writing – review & editing, Validation. **Eugene A. Olevsky:** Writing – review & editing, Supervision, Software, Conceptualization.

Declaration of competing interest

The authors declare that they have no known competing financial interests or personal relationships that could have appeared to influence the work reported in this paper.

Data availability

No data was used for the research described in the article.

Acknowledgements

The support of the National Science Foundation (Grants 2138421, 2119832 and 2119833) is gratefully acknowledged. The support of the US Department of Energy, Office of Basic Energy Sciences (Award No. SC0022244) is gratefully appreciated.

Data availability statement

The datasets used and/or analyzed during the current study are available from the corresponding author upon reasonable request.

References

[1] L.D.V.E. León, V.A. Escocio, L.L.Y. Visconte, J.C.J. Junior, E.B.A.V. Pacheco, Rotomolding and polyethylene composites with rotomolded lignocellulosic materials: a review, J. Reinf. Plast. Compos. 39 (2020) 459–472, https://doi.org/10.1177/0731684420916529.
[2] R. Shaker, D. Rodrigue, Rotomolding of thermoplastic elastomers based on low-density polyethylene and recycled natural rubber, Appl. Sci. 9 (2019) 1–20, https://doi.org/10.3390/app9245430.
[3] R.J. Crawford, J.L. Throne, Rotational Molding Technology, 2001.
[4] M. Sammouda, C.;. H.;Royere, A.;Maalej Belghith, Heat transfer in a rotating furnace of a solar sand!boiler at a 0999kW thermal concentration system, Renew. Energy. 17 (1999) 21–47.
[5] D.R. Van Puyvelde, Simulating the mixing and segregation of solids in the transverse section of a rotating kiln, Powder. Technol. 164 (2006) 1–12, https://doi.org/10.1016/j.powtec.2005.12.017.
[6] Y. Ninomiya, Parabolic mirror made by the rotation method : its fabrication and defects, 18 (1979).
[7] E... Olevsky, R... German, A. Upadhyaya, Effect of gravity on dimensional change during sintering—II. Shape distortion, Acta Mater. 48 (2000) 1167–1180, https://doi.org/10.1016/S1359-6454(99)00369-9.
[8] R.M. German, E. Torresani, E.A. Olevsky, Gravity-Induced Distortion During Liquid-Phase Sintering, Metall. Mater. Trans. A. (2023), https://doi.org/10.1007/s11661-023-07078-w.
[9] N. Satterlee, E. Torresani, E. Olevsky, J.S. Kang, Comparison of machine learning methods for automatic classification of porosities in powder-based additive manufactured metal parts, Int. J. Adv. Manuf. Technol. 120 (2022) 6761–6776, https://doi.org/10.1007/s00170-022-09141-z.
[10] E. Torresani, Influence of gravity on sintering of 3D- printed powder components, (2021). 10.1111/jace.18056.
[11] A. Mostafaei, A.M. Elliott, J.E. Barnes, F. Li, W. Tan, C.L. Cramer, P. Nandwana, M. Chmielus, Binder jet 3D printing—Process parameters, materials, properties, modeling, and challenges, Prog. Mater. Sci. 119 (2021) 100707, https://doi.org/10.1016/j.pmatsci.2020.100707.
[12] Sachs E.M., Haggerty J.S., Cima M.J., Williams P.A., n.d. 055. Three-dimensional printing techniques. US Patent 5,204.
[13] M. Zago, N.F.M. Lecis, M. Vedani, I. Cristofolini, Geometrical Issues in Design for Binder Jetting – The Effect of Anisotropic Dimensional Change on Sintering, in: Int. Conf. Des. Simulation, Manuf. Innov. Exch., 2022: pp. 410–421. 10g.1007/978-3-030-91234-5_42.
[14] M. Zago, N.F.M. Lecis, M. Vedani, I. Cristofolini, Dimensional and geometrical precision of parts produced by binder jetting process as affected by the anisotropic shrinkage on sintering, Addit. Manuf. 43 (2021) 102007, https://doi.org/10.1016/j.addma.2021.102007.
[15] S. Sadeghi, A. Shad, K. Abburi, N. Günther, V. Ploshikhin, Materials & Design Numerical simulation of shrinkage and deformation during sintering in metal binder jetting with experimental validation, Mater. Des. 216 (2022) 110490, https://doi.org/10.1016/j.matdes.2022.110490.

[16] A. Cabo Rios, T. Mishurova, L. Cordova, M. Persson, G. Bruno, E. Olevsky, E. Hryha, Ex-situ characterization and simulation of density fluctuations evolution during sintering of binder jetted 316L, Mater. Des. 238 (2024) 112690, https://doi.org/10.1016/j.matdes.2024.112690.
[17] E.A. Olevsky, Theory of sintering: from discrete to continuum, Mater. Sci. Eng. R Reports. 23 (1998) 41–100, https://doi.org/10.1016/S0927-796X(98)00009-6.
[18] A.C. Rios, E. Hryha, E. Olevsky, P. Harlin, A. Cabo, E. Hryha, E. Olevsky, P. Harlin, Sintering anisotropy of binder jetted 316L stainless steel : part I – sintering anisotropy, (2022). 10.1080/00325899.2021.2020485.
[19] A.C. Rios, E. Hryha, E. Olevsky, P. Harlin, A. Cabo, E. Hryha, E. Olevsky, P. Harlin, Sintering anisotropy of binder jetted 316L stainless steel : part II – microstructure evolution during sintering, (2022). 10.1080/00325899.2021.2020486.
[20] A. Cabo, E. Olevsky, E. Hryha, M. Persson, R.K. Bordia, Analytical models for initial and intermediate stages of sintering of additively manufactured stainless steel Acta Materialia Analytical models for initial and intermediate stages of sintering of additively manufactured stainless steel, Acta Mater. 249 (2023) 118822, https://doi.org/10.1016/j.actamat.2023.118822.
[21] E.A. Olevsky, R.M. German, Effect of gravity on dimensional change during sintering—I. Shrinkage anisotropy, Acta Mater. 48 (2000) 1153–1166, https://doi.org/10.1016/S1359-6454(99)00368-7.
[22] C.R. Alberto, E.A. Olevsky, E. Hryha, M. Persson, Modelling of δ-ferrite transformation effect on the sintering behaviour of 316L binder jetted components, WorldPM 2022 (2022).
[23] E.A. Olevsky, C. Garcia-Cardona, W.L. Bradbury, C.D. Haines, D.G. Martin, D. Kapoor, Fundamental aspects of spark plasma sintering: II. Finite element analysis of scalability, J. Am. Ceram. Soc. 95 (2012) 2414–2422, https://doi.org/10.1111/j.1551-2916.2012.05096.x.
[24] B.R.M. German, E.A. Olevsky, E. Torresani, D.L. Hernandez, Sintering experiments under way on International Space Station, (2019) 34–41.